European Journal of Radiology 116 (2019) 1–7

Contents lists available at ScienceDirect

European Journal of Radiology

journal homepage: www.elsevier.com/locate/ejrad

Research article

Predicting lymph node metastasis in pancreatobiliary cancer with magnetic resonance imaging: A prospective analysis

Ju Hee Lee[a,1], Sung-Sik Han[b,1], Eun Kyung Hong[c], Hwa Jin Cho[d], Jungnam Joo[e], Eun Young Park[d], Sang Myung Woo[f], Tae Hyun Kim[f], Woo Jin Lee[f], Sang-Jae Park[b,*]

[a] Department of Radiology, Center for Liver Cancer, National Cancer Center, Republic of Korea
[b] Department of Surgery, Center for Liver Cancer, National Cancer Center, Republic of Korea
[c] Department of Pathology, Center for Liver Cancer, National Cancer Center, Republic of Korea
[d] Department of Pathology, Inje University Busan Paik Hospital, Inje University College of Medicine, Busan, Republic of Korea
[e] Biometric Research Branch, Research Institute National Cancer Center, Republic of Korea
[f] Center for Liver Cancer, National Cancer Center, Republic of Korea

ARTICLE INFO

Keywords:
Biliary tract neoplasms
Pancreatic neoplasms
Lymph nodes
Diffusion magnetic resonance imaging

ABSTRACT

Objectives: To prospectively investigate the diagnostic potential of lymph node (LN) magnetic resonance (MR) imaging features.

Methods: A radiologist determined the maximum diameters in the short and long axes, shape, signal intensities on T1- and T2-weighted imaging, pattern of enhancement, and apparent diffusion coefficient (ADC) on diffusion-weighted MR images of LNs and annotated measurable (≥5 mm in short-axis diameter) LNs. Surgically harvested LNs were correlated with the pathologic findings. Univariable and multivariable generalized estimating equation analyses were performed to evaluate predictive power.

Results: Of 80 LNs, 29 (36.3%) were positive and 51 (63.7%) negative for metastasis. The mean short-axis diameter of metastatic LNs (10.59 ± 4.30 mm) was larger than that of benign LNs (7.96 ± 2.10 mm). The ADC was significantly ($P < 0.001$) lower in metastatic than non-metastatic LNs. The area under the curve (AUC) of a univariable model using only the mean ADC was 0.845 (95% confidence interval [CI], 0.743–0.927), and the mean-ADC cutoff value for predicting LN metastasis was 0.901×10^{-3} mm^2/s. The AUC of a multivariable model including round shape, heterogeneous enhancement, and the mean ADC was 0.917 (95% CI, 0.845–0.972), with a sensitivity, specificity, overall accuracy, and positive and negative predictive values of 89.7%, 82.4%, 85.0%, 74.3%, and 93.3%, respectively.

Conclusion: The short-axis diameter and ADC were different between benign and metastatic LNs in pancreatobiliary cancer. However, round shape, heterogeneous enhancement, and a low ADC value ($< 0.901 \times 10^{-3}$ mm^2/s) may be the most reliable diagnostic features of multiple metastatic LNs.

1. Introduction

Pancreatobiliary cancers are uncommon malignant tumors with poor prognosis. Surgical resection remains the only potentially curative therapy. Preoperative evaluation of prognostic parameters is important for a choice of radical surgery in pancreatobiliary cancers. Lymph node (LN) metastasis is a strong predictor of survival. In the new 8th edition of the American Joint Committee on Cancer (AJCC) Staging Manual [1], the N category has been refined for perihilar and distal bile duct, gallbladder, ampulla, and pancreas cancers. For these tumors, N1 is defined as 1–3, and N2 as 4 or more metastatic LNs. The number of metastatic LNs correlates with prognosis [2,3]. Therefore, the precise prediction of LN metastasis is crucial for clinical decision-making.

However, the preoperative diagnosis of LN metastasis is challenging with current imaging modalities, including computed tomography (CT) and magnetic resonance (MR) imaging. Frequently used criteria for LN metastasis include size > 10 mm in short-axis diameter, irregular margin, and central necrosis based on CT. However, albeit rarely, small LNs can also be metastatic [4]. MR with diffusion-weighted imaging is increasingly used for tumor detection and characterization. The apparent diffusion coefficient (ADC) is used to quantify diffusion-weighted imaging. The ADC is based on measuring the random motion

* Corresponding author.
E-mail addresses: spark@ncc.re.kr, jupiter3800@knou.ac.kr (S.-J. Park).
[1] Contributed equally to this study.

https://doi.org/10.1016/j.ejrad.2019.04.007
Received 19 December 2018; Received in revised form 26 March 2019; Accepted 12 April 2019

of water molecules and may reflect the pathologic changes within lymph nodes independently of node size [5–7]. ADC values have been used to characterize changes in various organs [5–12]. However, other studies have found no significant ADC differences between benign and metastatic nodes [13–16]. The technique of [^{18}F]-fluorodeoxyglucose positron emission tomography (FDG-PET) has insufficient spatial resolution to detect small LN metastases reliably [17,18].

To our knowledge, no studies have prospectively evaluated MR imaging features of LNs for radiologic–pathologic correlation in pancreatobiliary cancer. The aim of our study was to prospectively investigate the imaging characteristics of LNs detectable by 3 T MR with diffusion-weighted imaging and identify LN-metastasis-predictive features in pancreatobiliary cancer.

2. Material and methods

2.1. Patients

The study was approved by the Institutional Review Board. Written informed consent was obtained from the patients. The study was designed as a prospective single-center cohort study.

From April 2015 to March 2016, 90 consecutive patients who underwent elective surgery for suspected biliary or pancreatic malignancies on CT and/or MR were considered for inclusion. Exclusion criteria were neoadjuvant systemic therapy prior to surgery, age younger than 18 years, and no MR images within 30 days before surgery. We reviewed MR images and detected measurable LNs, which were defined as ≥5 mm in short-axis diameter to be able to measure ADC. A total of 40 patients underwent LN dissection for MR-measurable LNs. Four patients were excluded because of non-pancreatobiliary malignancies (n = 2) or unresectable LNs (n = 2) in final image analysis (Fig. 1).

2.2. MR imaging technique

MR examinations were performed on a 3.0 T MR system (Achieva 3.0TX; Philips Healthcare, Best, The Netherlands) with 16-channel phased-array receiver coils. Baseline MR imaging included axial T1-weighted dual-echo, axial, and coronal respiratory-triggered heavily T2-weighted sequences, coronal MR cholangiopancreatography (MRCP), and axial dynamic T1-weighted, three-dimensional spoiled gradient-echo sequences. Diffusion-weighted images were acquired using a respiratory-triggered single-shot echo-planar sequence with the following parameters: echo time (TE), 63 ms; repetition time (TR), 3000 ms; receiver bandwidth, 49 Hz per pixel; field of view (FOV), 350 × 350 mm; matrix, 116 × 116; slice thickness, 5 mm; intersection gap, 1 mm; and number of slices, 35. The images were obtained with *b* values of 0, 50, 400, and 800 s/mm [2]. For dynamic MR imaging, arterial phase (20–35 s), portal venous phase (60 s), and late phase (3 min and 5 min) images were obtained. The time for the arterial phase imaging was determined by using the MR fluoroscopic bolus detection technique. Gadoterate meglumine (Dotarem; Guerbet, Aulnay-Sous-Bois, France) at 0.1 mmol/kg of body weight was injected as a rapid bolus, followed immediately by a 20-mL saline flush through a power injector at 2 mL/s.

2.3. Image analysis

A board-certified abdominal radiologist (9 years of experience in abdominal MR imaging interpretation) reviewed MR images before surgery. The reader annotated all measurable (≥5 mm in short-axis diameter) LNs on the portal venous phase. The LNs were located in a commonly affected station and around the abdominal aorta within the standardized dissection area of pancreatobiliary cancers. To avoid confusion in the one-to-one comparison between radiological and surgical findings, we limited the size of LNs to ≥5 mm in short-axis diameter and a maximum of 10 annotated LNs per patient. The reader also

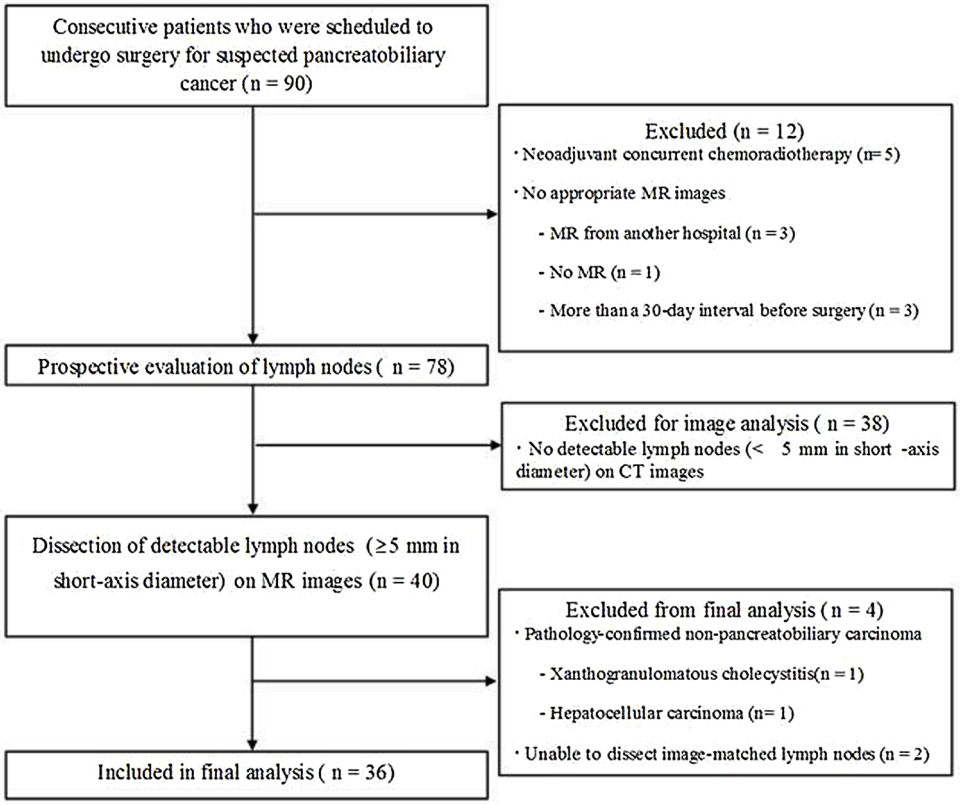

Fig. 1. Flow diagram of patient selection.

documented the LN location according to the Classification of Biliary Tract Cancers by the Japanese Society of Hepato-Biliary-Pancreatic Surgery [19] as follows: LN#8, common hepatic artery; LN#9, celiac artery; LN#12, hepatoduodenal ligament; LN#13, posterior surface of the head of the pancreas; LN#16, paraaortic. MR images with classified annotated LNs (e.g., LN#8-1, LN#12-2) were reviewed preoperatively by the radiologist and surgeon in consensus.

The maximum diameter of each LN in short axis and long axis at the right angle were measured on the portal venous phase of MR images. The short/long axis ratio was calculated. The LN shape (oval or round) was defined as follows: oval shape, less than 0.8 of the short/long axis ratio; or round shape, equal to or more than 0.8 of that ratio. The signal intensity of the LNs compared with that of the liver was assessed on T1- and T2-weighted images. The enhancement patterns of the LNs were classified into homogeneous and heterogeneous enhancement on portal venous phase images.

For quantitative analysis, each annotated LN was identified on the corresponding diffusion-weighted image. A region of interest (ROI) for each LN was drawn on a diffusion-weighted image obtained with a *b* value of 800 s/mm [2]. Circular or ovoid ROI were applied to include almost the entire area of the visible LN while avoiding the most peripheral portions to exclude partial volume effects of adjacent extralesional tissue. The ROI was copied to the ADC map, and the mean ADC value of three measurements was calculated by the radiologist.

2.4. Surgery and histopathology

All patients underwent radical resection with lymphadenectomy or explorative laparotomy with lymph node dissection. LN dissection was performed as a usual manner according to the tumor location. The most common site of LN dissection is common hepatic artery, celiac artery, hepatoduodenal ligament and retropancreatic area. Paraaortic LN sampling was performed if metastasis was highly suspected. The surgeons reviewed the MR images with the radiologist before surgery to precisely localize the annotated LNs intraoperatively. They used the major vascular structures (e.g., common hepatic artery, portal vein, gastroduodenal artery, celiac artery, inferior vena cava, and aorta) and common bile duct as landmarks to localize the annotated LNs. By measuring the distance from these landmarks and constructing a 3-dimensional (3D) relationship with these anatomical structures, the surgeons could exactly identify the annotated LNs intraoperatively and dissect them (Fig. 2) separately from the main tumor. On histopathologic examination, the 3D diameter of the dissected LN was analyzed to correlate with the image. The LN was sliced with a maximum thickness of 3 mm and stained with hematoxylin-eosin. The sizes of the metastatic foci were measured. The histopathologic results were used as a standard reference.

2.5. Statistical analysis

LN imaging features were summarized as means ± standard deviation for continuous and counts (proportions) for categorical variables, respectively. The generalized estimating equation (GEE) method was used to assess the correlation among multiple LNs in a patient. The working correlation matrix was assumed to be exchangeable so that the correlation of multiple observed variables in a patient was constant. Univariable and multivariable GEE analyses based on the logistic model were performed to predict LN metastasis. The model included short- and long-axis diameters, shape, T1- and T2-weighted imaging SIs, enhancement pattern, and the ADC. Intraobserver agreement of ADC measurement were assessed by the Bland–Altman plot and intraclass correlation coefficient (ICC). Backward variable elimination was considered, and the model with the smallest quasi-likelihood under the independence model criterion (QICu) was chosen as the final model. The discrimination ability of the model was measured by the area under the curve (AUC). All statistical analyses were performed using SAS version 9.4 (SAS Institute Inc., Cary, NC, USA) and R project version 3.3.3. *P*-values less than 0.05 were considered significant.

3. Results

A total of 36 patients (24 men, 12 women; median age, 69 years; range, 43–79 years) were included for final analysis, and 80 LNs in total were evaluated. The cases included distal bile duct carcinoma [12], hilar cholangiocarcinoma [5], intrahepatic cholangiocarcinoma [5], and gallbladder, ampullary, and pancreatic carcinoma (4, 5, and 5, respectively).

The median time interval between preoperative MR imaging and surgery was 6 days (interquartilerange,9). The number of evaluated LNs in a patient was 1–7. Twenty-nine LNs, in 13 patients, were metastatic and 51 LNs were pathologically benign. The LN imaging features are summarized in Table 1. The locations of the 80 LNs were as follows: 22 (5 metastatic and 17 benign) in LN#8; 2 (1 metastatic and 1 benign) in LN#9; 44 (16 metastatic and 28 benign) in LN#12; 1 metastatic node in LN#13, and 11 (6 metastatic and 5 benign) in LN#16.

We used the mean ADC because ADC measurements were highly reproducible as evaluated by the ICC and Bland–Altman plot (ICC 0.93 [0.90–0.95], Supplementary Fig. 1). The ADC was significantly ($P < 0.001$) lower in metastatic ($0.8220 \times 10^{-3} \pm 0.1319 \times 10^{-3}$ mm^2/s) than non-metastatic LNs ($1.0310 \times 10^{-3} \pm 0.1674 \times 10^{-3}$ mm^2/s). Univariable analyses showed that short-axis diameter, heterogeneous enhancement, and the mean ADC were associated with LN metastasis. A multivariable model including round shape, heterogeneous enhancement, and mean ADC was chosen as the best model based on the QICu criterion (Table 2).

The AUC of a univariable model using the mean ADC was 0.845 (95% confidence interval [CI] calculated by 2000 bootstrap, 0.743–0.927) (Fig. 3). The predicted probability of LN metastasis at the maximum summation of sensitivity and specificity was 0.351. Based on this probability, the mean-ADC cutoff value for predicting LN metastasis was calculated to be 0.901×10^{-3} mm^2/s. The sensitivity, specificity, overall accuracy, positive predictive value (PPV), and negative predictive value (NPV) for differentiating metastatic from non-metastatic LNs based on this threshold were 79.3%, 78.4%, 78.8%, 67.7%, and 87.0%, respectively. The AUC of a multivariable model with round shape, heterogeneous enhancement, and the mean ADC was 0.917 (95% CI calculated by 2000 bootstrap, 0.845–0.972). The sensitivity, specificity, overall accuracy, PPV, and NPV of the multivariable model were 89.7%, 82.4%, 85.0%, 74.3%, and 93.3%, respectively.

4. Discussion

LN metastasis is a well-known poor prognostic factor in pancreatobiliary cancers and surgery of these cancers has high morbidity and mortality among the gastrointestinal cancers. Therefore, even when the primary tumor is resectable, the upfront surgery may not be indicated if the patients have highly suspicious LN metastasis on preoperative imaging studies because the patients are usually old and have combined cardio-pulmonary, renal, or cerebrovascular comorbidities. Therefore, the precise prediction of LN metastasis is crucial for clinical decision-making.

We investigated the diagnostic usefulness of diffusion-weighted MR imaging, quantified by ADC values, in distinguishing metastatic from non-metastatic LNs in pancreatobiliary cancer. Little literature exists on LN metastasis diagnosis with MR imaging in pancreatobiliary cancer. Unlike previous studies [5,13], ours prospectively examined nodes that appeared benign, malignant, or had uncertain appearance, and pathologic results for all nodes were obtained.

The normal sizes of upper abdominal LNs range from 6 to 20 mm depending on the node location, with the upper normal-size limits varying from 7 to 10 mm [20]. We found statistically significant difference in the short-axis diameter between benign (7.96 ± 2.10 mm)

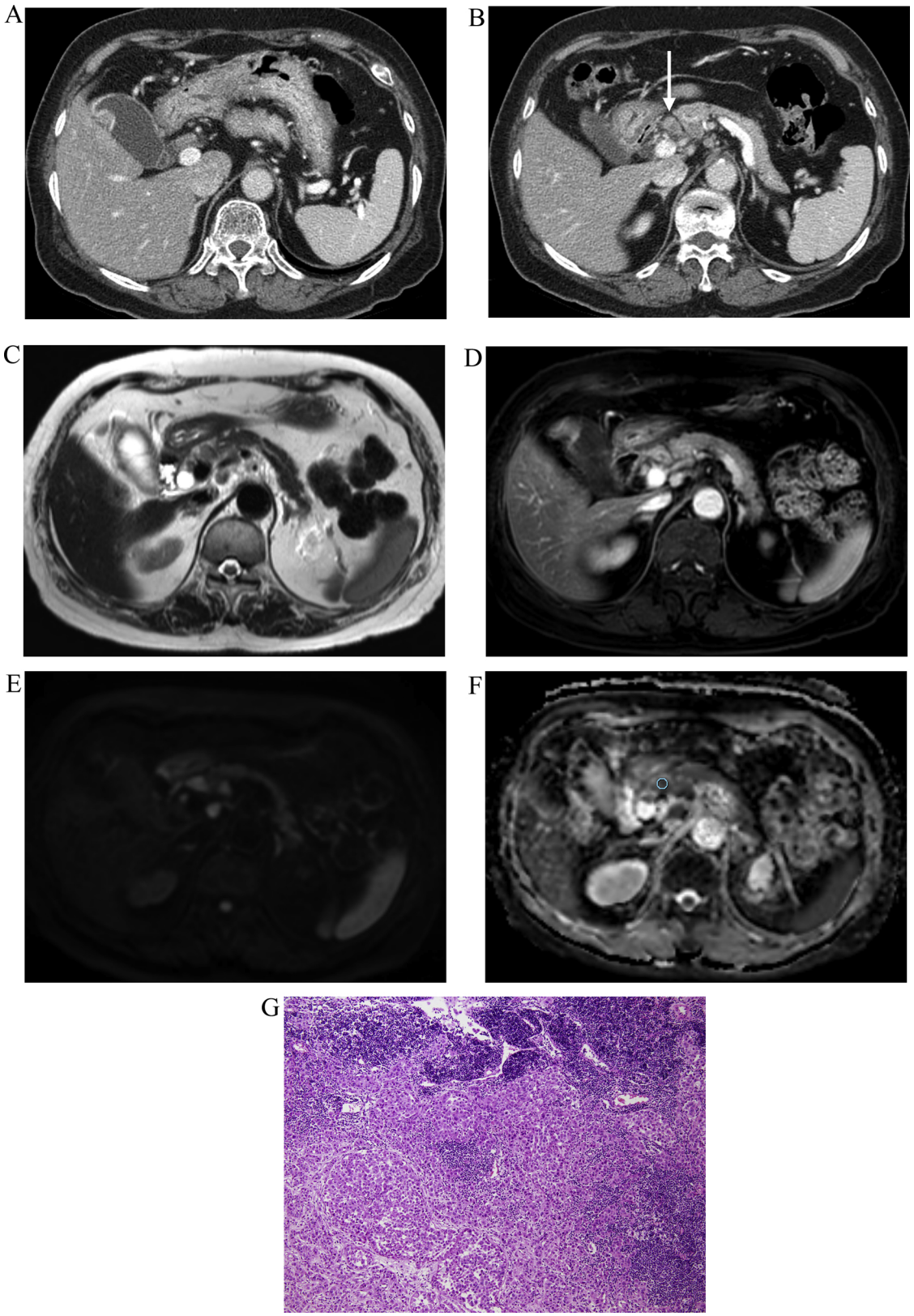

Fig. 2. Imaging and histologic findings of a 71-year-old woman who underwent radical cholecystectomy for gallbladder carcinoma (stage pT2N2). (A) Axial contrast-enhanced computed tomography showed a mass at the gallbladder fundus and (B) an enlarged lymph node (arrow) with heterogeneous enhancement along the common hepatic artery. The node demonstrated high signal intensity on axial T2-weighted imaging (C) and heterogeneous enhancement on portal venous phase magnetic resonance imaging (D). (E) A diffusion-weighted image (with a *b* value of 800 s/mm^2) shows the same lymph node with high signal intensity. (F) The corresponding apparent diffusion coefficient (ADC) map shows a low mean ADC value (0.861×10^{-3} mm^2/s) in the node (circumscribed area). (G) Histologic analysis revealed that the lymph node was almost entirely replaced by metastatic infiltration (original magnification, × 100).

Table 1
Magnetic Resonance Image Features of Non-metastatic and Metastatic Lymph Nodes (LNs).

	Non-metastatic LN (N = 51)	Metastatic LN (N = 29)	*P*-value*
Long axis diameter (mm)	16.24 ± 5.75	16.72 ± 6.13	0.164
Short axis diameter (mm)	7.96 ± 2.10	10.59 ± 4.30	0.007
Shape			1.000
Oval	50 (98.0)	18 (62.1)	
Round (ratio of short to long axis diameter > 0.8)	1 (2.0)	11 (37.9)	
SI on T1WI			N/A†
Iso	2 (3.9)	0 (0.0)	
Low	49 (96.1)	29 (100.0)	
SI on T2WI			0.502
High	46 (90.2)	26 (89.7)	
Iso	5 (9.8)	3 (10.3)	
Pattern of enhancement			< 0.001
Heterogeneous	1 (2.0)	14 (48.3)	
Homogeneous	50 (98.0)	15 (51.7)	
Mean ADC	1.0310 ± 0.1674	0.8220 ± 0.1319	< 0.001

ADC, apparent diffusion coefficient; SI, signal intensity; WI, weighted imaging.
* Calculated by the generalized estimating equation.
† *P* value cannot be estimated by GEE method, because there was no value according to the metastatic case with iso SI.

and metastatic (10.59 ± 4.30 mm) LNs in univariable analyses. However, the diameter was not chosen as the best model in multivariable analyses on QICu criterion, reflecting correlation among multiple LNs in a patient. Most (58.6% [17 of 29]) metastatic LNs were ≤10 mm in size. When the size criterion of 1 cm of short-axis diameter was applied, it yielded a sensitivity of 51.7%, specificity of 80.4%, accuracy of 70%, PPV of 60%, and NPV of 74.6%. Morimoto et al. (2008) analyzed metastatic LNs in biliary cancer and proposed the cutoff size for positive LNs of > 7.5 mm or > 10 mm with sensitivities of 60.8% and 47.1%, and specificities of 69.7% and 79.3%, respectively [4]. The size of a metastatic LN and its metastatic area percentage were positively correlated [4]. We excluded nodes < 5 mm in short-axis diameter; however, some of them were metastatic. Most small metastatic LNs were found in patients with pancreatic cancer, in the peripancreatic or peritumoral area. In these cancers, detectable nodes were mostly located in LN#8 and LN#12, whereas peripancreatic node detection was poor in our study. This observation may indicate that the pancreatic cancers often had small-sized metastatic nodes in the peritumoral/peripancreatic area, consistent with the LN downstaging rate to cN0 being approximately 38%, with an NPV of 49.8% for LN metastasis [21]. Therefore, nodal size may not be a reliable criterion for LN metastasis in pancreatobiliary cancer, and the sizes of peritumoral nodes should be interpreted with caution.

Nodal necrosis is a well-known feature predicting LN metastasis that results in heterogeneous enhancement. Our study confirmed this finding and demonstrated that most necrotic nodes are metastatic. However, necrotic nodes can also be benign in conditions such as tuberculosis, and are not reliable for metastasis diagnosis. When tumor cells infiltrate an LN, the node becomes enlarged and round. We measured the short/long axis ratio to assess the shape objectively. Although the shape determined by these parameters was not significantly different between benign and metastatic nodes, adding shape to the multivariable model decreased the QICu, and a multivariable model including round shape, ADC, and heterogeneous enhancement showed improved performance.

Normal LNs show relatively restricted diffusion because of high cellular densities and are well-visualized while surrounding fat tissue is suppressed on diffusion-weighted imaging [22]. Therefore, diffusion-weighted imaging is a valuable tool for LN identification and characterization. Metastatic LNs may further restrict diffusion because the increased cell number and nucleocytoplasmic ratio, and decreased extracellular space in malignancy limit water diffusion. In our study, the mean ADC of the metastatic LNs was significantly lower than that of the benign LNs. The mean-ADC cutoff was 0.901×10^{-3} mm^2/s, and the AUC using mean ADCs was 0.845, with a sensitivity, specificity, and an NPV of 79.3%, 78.4%, and 87.0%, respectively. Many studies have reported the usefulness of ADCs in differentiating between benign and malignant nodes [6,23–28]. However, the ADC cutoff values in these studies were both variable and different from ours. Furthermore, Heijnen et al. (2013) reported the mean ADC to be higher for benign than malignant nodes in rectal cancer, although the difference was not statistically significant [14]. These discrepancies may be explained by other studies investigating different cancers (i.e., head/neck, esophageal, cervical, and rectal) and histopathological types (i.e., adenocarcinoma and squamous cell carcinoma). Consistent with this explanation, the ADC was not reproducible in the same cancer type, depending on patient characteristics, preoperative chemoradiotherapy, and MR protocol [14,29]. Therefore, ADC standardization is necessary. Further study is required for the general application of an LN characteristic threshold in different organs.

We measured ADCs to draw ROIs on diffusion-weighted images and ADC maps. The ADC is affected by many factors, including tissue diffusivity, regional gradient, and the individual magnetic environment [30], which is considered an inherent limitation of diffusion-weighted imaging. ADC measurement for small LNs is potentially limited by susceptibility to artifacts and image distortions. In addition, partial volume averaging can occur in diffusion-weighted imaging, which uses 5-mm-thick slices. Since LNs are relatively small and have an elliptical

Table 2
Univariable and Multivariable Analyses Using the Generalized Estimation Equation.

	Univariable			Multivariable (QICu = 60.472)	
	OR (95% CI)	*P*-value	QICu	OR (95% CI)	*P*-value
Long axis diameter (mm)	1.04 (0.98–1.09)	0.164	109.955		
Short axis diameter (mm)	1.16 (1.04–1.29)	0.007	100.769		
Shape					
Oval	1			1	
Round	1.00 (0.23–4.41)	1.000	109.567	9.59 (0.72–127.70)	0.087
SI on T2WI					
High	1				
Iso	0.72 (0.27–1.89)	0.502	109.732		
Pattern of enhancement					
Homogeneous	1			1	
Heterogeneous	4.53 (2.13–9.65)	< 0.001	90.311	24.62 (4.16–145.82)	< 0.001
Mean ADC*10	0.44 (0.29–0.69)	< 0.001	79.023	0.35 (0.17–0.74)	0.006

ADC, apparent diffusion coefficient; OR, odds ratio; QICu, quasi-likelihood under the independence model criterion; SI, signal intensity; WI, weighted imaging.

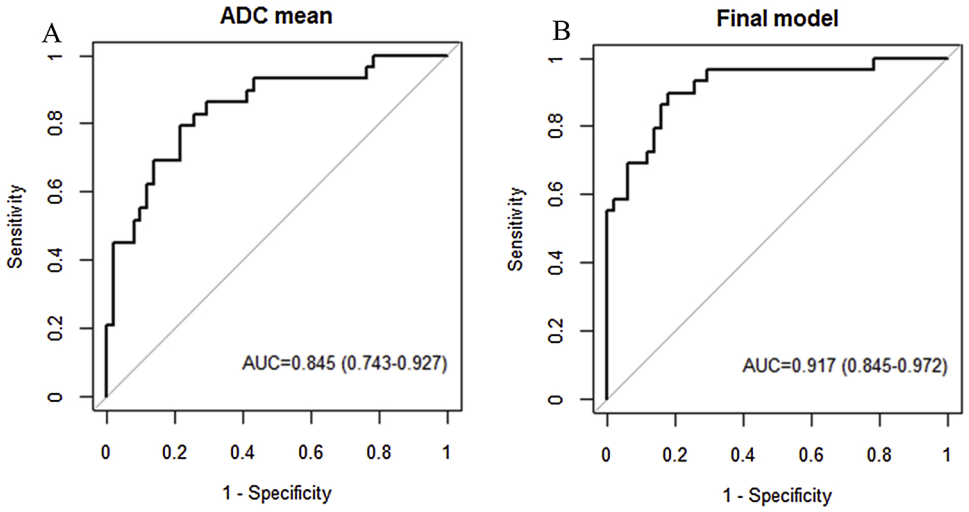

Fig. 3. Receiver operating characteristic (ROC) curves based on a univariable model using only the mean apparent diffusion coefficient (ADC) (A) and a multivariable model including shape, pattern of enhancement, and the mean ADC (B) for the differentiation of metastatic from non-metastatic lymph nodes.

shape, we selected nodes > 5 mm in diameter and drew an ROI covering the entire node while avoiding adjacent fat or other tissues to minimize the effect of partial volume averaging. We achieved good image quality by using a 3 T MR scanner with high resolution: the ICC of triplicate ADC measurements was extremely high.

Our study has limitations. First, the numbers of included patients and metastatic LNs were small, mainly because of the strict inclusion criteria. For ROI measurements on ADC maps, we included only LNs ≥5 mm in short-axis diameter, and many small LNs in the peripancreatic area were excluded. In addition, we limited the number of LNs per patient to 10, which was determined by consensus with the surgeons. Large-scale prospective studies are needed to confirm our findings. Second, not all para-aortic small LNs were included because we limited the study only to the standardized dissection area for pancreatobiliary cancers. When a para-aortic LN was suspected to be metastatic, it was included in the study after discussion with the surgeon.

In conclusion, we found that short-axis diameter and ADC value of LNs are significant criteria to differentiate metastatic from benign nodes in pancreatobiliary cancer. However, when reflecting correlation among multiple LNs in a patient, round shape, heterogeneous enhancement, and low ADC values may be the most reliable features for metastatic LN diagnosis. Therefore, diffusion-weighted MR imaging may play an important role in differentiating LN metastasis preoperatively.

Conflicts of interest

There are no conflicts of interest.

Acknowledgements

The present study was supported by grants from the National Cancer Center, Korea (grant numbers 1510720-1 and 1711270-1).

Appendix A. Supplementary data

Supplementary material related to this article can be found, in the online version, at doi:https://doi.org/10.1016/j.ejrad.2019.04.007.

References

[1] M.B. Amin, S. Edge, F. Greene, D.R. Byrd, R.K. Brookland, M.K. Washington, et al., AJCC Cancer Staging Manual, 8th ed., Springer International Publishing, New York, 2017.
[2] M. Kiriyama, T. Ebata, T. Aoba, Y. Kaneoka, T. Arai, Y. Shimizu, et al., Prognostic impact of lymph node metastasis in distal cholangiocarcinoma, Br. J. Surg. 102 (4) (2015) 399–406.
[3] O. Strobel, U. Hinz, A. Gluth, T. Hank, T. Hackert, F. Bergmann, et al., Pancreatic adenocarcinoma: number of positive nodes allows to distinguish several N categories, Ann. Surg. 261 (5) (2015) 961–969.
[4] H. Morimoto, T. Ajiki, T. Ueda, H. Sawa, T. Fujita, I. Matsumoto, et al., Histological features of lymph node metastasis in patients with biliary tract cancer, J. Surg. Oncol. 97 (5) (2008) 423–427.
[5] K. Holzapfel, J. Gaa, E.C. Schubert, M. Eiber, J. Kleeff, E.J. Rummeny, et al., Value of diffusion-weighted MR imaging in the diagnosis of lymph node metastases in patients with cholangiocarcinoma, Abdom. Radiol. (NY) 41 (10) (2016) 1937–1941.
[6] J.K. Kim, K.A. Kim, B.W. Park, N. Kim, K.S. Cho, Feasibility of diffusion-weighted imaging in the differentiation of metastatic from nonmetastatic lymph nodes: early experience, J. Magn. Reson. Imaging 28 (3) (2008) 714–719.
[7] K. Yamaguchi, D. Schacht, T. Nakazono, H. Irie, H. Abe, Diffusion weighted images of metastatic as compared with nonmetastatic axillary lymph nodes in patients with newly diagnosed breast cancer, J. Magn. Reson. Imaging 42 (3) (2015) 771–778.
[8] A.A. Razek, G. Gaballa, A. Denewer, N. Nada, Invasive ductal carcinoma: correlation of apparent diffusion coefficient value with pathological prognostic factors, NMR Biomed. 23 (6) (2010) 619–623.
[9] S.K. Jeh, S.H. Kim, H.S. Kim, B.J. Kang, S.H. Jeong, H.W. Yim, et al., Correlation of the apparent diffusion coefficient value and dynamic magnetic resonance imaging findings with prognostic factors in invasive ductal carcinoma, J. Magn. Reson. Imaging 33 (1) (2011) 102–109.
[10] F. Fornasa, M.V. Nesoti, C. Bovo, M.G. Bonavina, Diffusion-weighted magnetic resonance imaging in the characterization of axillary lymph nodes in patients with breast cancer, J. Magn. Reson. Imaging 36 (4) (2012) 858–864.
[11] M. Iima, M. Kataoka, R. Okumura, K. Togashi, Detection of axillary lymph node metastasis with diffusion-weighted MR imaging, Clin. Imaging 38 (5) (2014) 633–636.
[12] T. Seber, E. Caglar, T. Uylar, N. Karaman, E. Aktas, B.K. Aribas, Diagnostic value of diffusion-weighted magnetic resonance imaging: differentiation of benign and malignant lymph nodes in different regions of the body, Clin. Imaging 39 (5) (2015) 856–862.
[13] J. Promsorn, W. Soontrapa, K. Somsap, N. Chamadol, P. Limpawattana, M. Harisinghani, Evaluation of the diagnostic performance of apparent diffusion coefficient (ADC) values on diffusion-weighted magnetic resonance imaging (DWI) in differentiating between benign and metastatic lymph nodes in cases of cholangiocarcinoma, Abdom. Radiol. (2018) 1–9, https://doi.org/10.1007/s00261-018-1742-6.
[14] L.A. Heijnen, D.M. Lambregts, D. Mondal, M.H. Martens, R.G. Riedl, G.L. Beets, et al., Diffusion-weighted MR imaging in primary rectal cancer staging demonstrates but does not characterise lymph nodes, Eur. Radiol. 23 (12) (2013) 3354–3360.
[15] H.K. Lim, J.H. Lee, H.J. Baek, N. Kim, H. Lee, J.W. Park, et al., Is diffusion-weighted MRI useful for differentiation of small non-necrotic cervical lymph nodes in patients with head and neck malignancies? Korean J. Radiol. 15 (6) (2014) 810–816.
[16] R.J. Schipper, M.L. Paiman, R.G. Beets-Tan, P.J. Nelemans, B. de Vries, E.M. Heuts, et al., Diagnostic performance of dedicated axillary T2- and diffusion-weighted MR imaging for nodal staging in breast cancer, Radiology 275 (2) (2015) 345–355.
[17] S. Sironi, A. Buda, M. Picchio, P. Perego, R. Moreni, A. Pellegrino, et al., Lymph node metastasis in patients with clinical early-stage cervical cancer: detection with integrated FDG PET/CT, Radiology 238 (1) (2006) 272–279.
[18] S. Kobayashi, H. Nagano, H. Hoshino, H. Wada, S. Marubashi, H. Eguchi, et al., Diagnostic value of FDG-PET for lymph node metastasis and outcome of surgery for biliary cancer, J. Surg. Oncol. 103 (3) (2011) 223–229.

[19] M. Miyazaki, M. Ohtsuka, S. Miyakawa, M. Nagino, M. Yamamoto, N. Kokudo, et al., Classification of biliary tract cancers established by the Japanese Society of Hepato-Biliary-Pancreatic Surgery: 3(rd) English edition, J. Hepatobiliary Pancreat. Sci. 22 (3) (2015) 181–196.
[20] R.E. Dorfman, M.B. Alpern, B.H. Gross, M.A. Sandler, Upper abdominal lymph nodes: criteria for normal size determined with CT, Radiology 180 (2) (1991) 319–322.
[21] H.S. Tran Cao, Q. Zhang, Y.H. Sada, E.J. Silberfein, C. Hsu, G. Van Buren 2ndet al., Value of lymph node positivity in treatment planning for early stage pancreatic cancer, Surgery 162 (3) (2017) 557–567.
[22] T.C. Kwee, T. Takahara, R. Ochiai, R.A. Nievelstein, P.R. Luijten, Diffusion-weighted whole-body imaging with background body signal suppression (DWIBS): features and potential applications in oncology, Eur. Radiol. 18 (9) (2008) 1937–1952.
[23] M. Sumi, N. Sakihama, T. Sumi, M. Morikawa, M. Uetani, H. Kabasawa, et al., Discrimination of metastatic cervical lymph nodes with diffusion-weighted MR imaging in patients with head and neck cancer, AJNR Am. J. Neuroradiol. 24 (8) (2003) 1627–1634.
[24] A.D. King, A.T. Ahuja, D.K. Yeung, D.K. Fong, Y.Y. Lee, K.I. Lei, et al., Malignant cervical lymphadenopathy: diagnostic accuracy of diffusion-weighted MR imaging, Radiology 245 (3) (2007) 806–813.
[25] E.I. Akduman, A.J. Momtahen, N.C. Balci, N. Mahajann, N. Havlioglu, M.K. Wolverson, Comparison between malignant and benign abdominal lymph nodes on diffusion-weighted imaging, Acad. Radiol. 15 (5) (2008) 641–646.
[26] G. Lin, K.C. Ho, J.J. Wang, K.K. Ng, Y.Y. Wai, Y.T. Chen, et al., Detection of lymph node metastasis in cervical and uterine cancers by diffusion-weighted magnetic resonance imaging at 3T, J. Magn. Reson. Imaging 28 (1) (2008) 128–135.
[27] G. Nakai, M. Matsuki, Y. Inada, F. Tatsugami, M. Tanikake, I. Narabayashi, et al., Detection and evaluation of pelvic lymph nodes in patients with gynecologic malignancies using body diffusion-weighted magnetic resonance imaging, J. Comput. Assist. Tomogr. 32 (5) (2008) 764–768.
[28] A. Sakurada, T. Takahara, T.C. Kwee, T. Yamashita, S. Nasu, T. Horie, et al., Diagnostic performance of diffusion-weighted magnetic resonance imaging in esophageal cancer, Eur. Radiol. 19 (6) (2009) 1461–1469.
[29] O. Yasui, M. Sato, A. Kamada, Diffusion-weighted imaging in the detection of lymph node metastasis in colorectal cancer, Tohoku J. Exp. Med. 218 (3) (2009) 177–183.
[30] M. Hoehn-Berlage, M. Eis, B. Schmitz, Regional and directional anisotropy of apparent diffusion coefficient in rat brain, NMR Biomed. 12 (1) (1999) 45–50.